DALTON

Ab-initio X-ray powder diffraction structural characterization of co-ordination compounds: polymeric $[\{MX_2(bipy)\}_n]$ complexes (M = Ni or Cu; X = Cl or Br; bipy = 4,4′-bipyridyl)†

Norberto Masciocchi,*[a] Paolo Cairati,[a] Lucia Carlucci,[a] Gianni Mezza,[b] Gianfranco Ciani[a] and Angelo Sironi*[a]

[a] *Dipartimento di Chimica Strutturale e Stereochimica Inorganica, Università di Milano, via Venezian 21, 20133 Milano, Italy*

[b] *Centro C.N.R. per la Sintesi e la Struttura dei Composti di Coordinazione in Bassi Stati di Ossidazione, via Venezian 21, 20133 Milano, Italy*

In the absence of crystals of suitable quality, the crystal structures of five $[MX_2(bipy)]$ (M = Ni or Cu; X = Cl or Br; bipy = 4,4′-bipyridyl) phases were determined, *ab initio*, from powder diffraction data. The nickel compounds contain symmetrically bridging halides and *trans*-D_{4h} octahedrally co-ordinated metal atoms; on the contrary, the co-ordination about the copper atoms in $[CuBr_2(bipy)]$ is square planar, with long Cu · · · Br contacts in the axial direction, due to Jahn–Teller distortion. Interestingly, $[CuCl_2(bipy)]$ is dimorphic; both in the orthorhombic and in the monoclinic phases, the copper co-ordination is substantially square planar as in the bromide analogue, but none of the two phases is isomorphous to it.

Linear bidentate N,N′-donor compounds have been extensively used in recent times with the aim of obtaining polymeric frameworks having potential properties in different areas of material science, such as electrical conductivity,[1] magnetism,[2] photomechanical behaviour,[3] clathration ability and catalysis.[4] On varying the lengths of these molecular rods and the salts employed a number of polymeric systems have been isolated, displaying different and interesting geometries. Among them, 4,4′-bipyridyl (hereafter bipy) has proven to be able to give one-dimensional polymers,[5] two-dimensional layers,[2c,4,6] eventually interwoven,[7] and three-dimensional frameworks exhibiting interpenetration of nets of the super-diamond type[8,9] or more complex ones.[10]

The first complexes of the transition metals with 4,4′-bipyridyl were prepared in the late '60s and their structures suggested mainly on the basis of IR data.[11,12] In particular, for the dihalide adducts $[MX_2(4,4'\text{-bipy})]$ (M = Mn^{2+}, Fe^{2+}, Co^{2+}, Ni^{2+}, Cu^{2+}, Zn^{2+}, Cd^{2+} or Hg^{2+}) two-dimensional polymeric six-co-ordinate structures, with bridging 4,4′-bipyridyl and halides, were proposed, except for that of Zn^{2+}, which was considered to be a one-dimensional polymeric tetrahedral complex.[12] These compounds are normally obtained as powdered materials and are typically insoluble in all common organic solvents and, therefore, difficult to crystallize. While, for the related polymeric MX_2 adducts of pyrazines, two single-crystal structure determinations have been reported, namely $[NiBr_2(dmpyz)]$[13] (dmpyz = 2,5-dimethylpyrazine) (based on square-planar co-ordination) and $[CuBr_2(pyz)]$, crystals of which have been obtained only recently by gel crystallization,[14] to our knowledge no structural report has so far appeared for the 4,4′-bipyridyl derivatives. It seemed therefore interesting to ascertain the detailed structural features of the $[MX_2(bipy)]$ species by diffraction methods.

While molecular species can normally be studied by conventional single-crystal methods, many intractable polymeric complexes can only be obtained as microcrystalline materials; therefore, all structural information must be extracted from powdered samples only. Accordingly, we have recently studied the polymeric forms of $[Ru(CO)_4]$,[15] $[MX_2(pydz)]$ (M = Mn, Fe, Co, Ni or Cu; X = Cl or Br; pydz = pyridazine),[16] pyrazolates[17] and imidazolates of Cu and Ag,[18] the crystal structures of which were successfully solved, and later refined, from standard laboratory X-ray powder diffraction data. Therefore, a complete structure determination, from powder diffraction data *only*, of the $[MX_2(bipy)]$ (M = Ni or Cu, X = Cl or Br) phases was undertaken and the results are reported here.

Experimental

General comments

All the reagents and solvents employed were commercially available high-grade purity materials: 4,4′-bipyridyl, $NiCl_2 \cdot 6H_2O$, $NiBr_2 \cdot 3H_2O$, $CuCl_2 \cdot 2H_2O$ and $CuBr_2$ (Fluka Chemie). They were used as supplied, without further purification. Elemental analyses were carried out at the Microanalytical Laboratory of this University.

Physical measurements

Infrared spectra were recorded on a Perkin-Elmer 371 grating spectrophotometer (range 4000–600 cm^{-1}) in KBr pellets. Room-temperature magnetic susceptibilities were measured on an MSB-AUTO (Sherwood Scientific) magnetic balance. Diamagnetic corrections were estimated from Pascal's constants. Thermogravimetric measurements were performed with the aid of Perkin-Elmer TGA 7 equipment.

Syntheses

All products were obtained by addition of an ethanolic solution of 4,4′-bipyridyl to an aqueous solution of the appropriate salt at room temperature in the molar ratio 1 : 1. The preparation of $[\{CuBr_2(bipy)\}_n]$ is described, the synthesis of the other species being accomplished on the same lines. Repeated syntheses under slightly different conditions (concentration, temperature and diffusion control) always afforded products of limited

† *Supplementary data available* (No. SUP 57141, 51 pp.): reflection indices, *d* spacings and structure factors. See Instructions for Authors, *J. Chem. Soc., Dalton Trans.*, 1996, Issue 1.

Non-SI unit employed: $\mu_B \approx 9.27 \times 10^{-24}$ J T^{-1}.

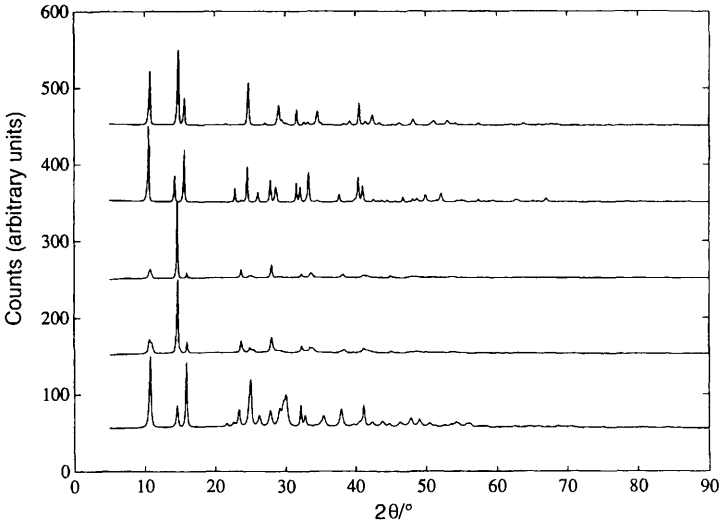

Fig. 1 Raw diffraction data for the five (poly)crystalline phases discussed in the text, in the 5 < 2θ < 90° range. Top to bottom: **1a**, **1b**, **2a**(α), **2a**(β) and **2b**

crystallinity, for which special care in the diffraction data analysis was need (see later).

[$CuBr_2$(bipy)] 2b. An ethanolic solution (3 cm^3) of 4,4′-bipyridyl (0.428 g, 2.74 mmol) was added to an aqueous solution (15 cm^3) of $CuBr_2$ (0.611 g, 2.74 mmol). The mixture immediately changed to green and a precipitate separated. It was filtered off (Whatman paper, pore size 0.2 mm) and dried in air (yield 90%) (Found: C, 31.65; H, 2.10; N, 7.00. Calc. for $C_{10}H_8Br_2CuN_2$: C, 31.65; H, 2.10; N, 7.40%). The green complex displays μ_{eff} = 1.65 μ_B at 294 K. Main 4,4′-bipyridyl IR bands (cm^{-1}): 1608vs, 1491s, 1414s, 1224vs, 1077vs, 813vs, 723s and 643s.

[$NiCl_2$(bipy)] 1a. Reagent: $NiCl_2 \cdot 6H_2O$. Yield 62% (Found: C, 42.95; H, 2.80; N, 9.90. Calc. for $C_{10}H_8Cl_2N_2Ni$: C, 42.05; H, 2.80; N, 9.80%). The pale green complex displays μ_{eff} = 3.15 μ_B at 294 K. Main 4,4′-bipyridyl IR bands (cm^{-1}): 1604vs, 1491s, 1414vs, 1220vs, 1077s, 1050m, 1010m, 853w, 810vs, 726vs and 636vs.

[$NiBr_2$(bipy)] 1b. Reagent: $NiBr_2 \cdot 3H_2O$. Yield 74% (Found: C, 31.80; H, 1.90; N, 7.30. Calc. for $C_{10}H_8Br_2N_2Ni$: C, 32.05; H, 2.15; N, 7.50%). The pale green complex displays μ_{eff} = 3.11 μ_B at 294 K. Main 4,4′-bipyridyl IR bands (cm^{-1}): 1611vs, 1491m, 1414m, 1120s, 1071m, 1050m, 1007m, 803vs, 723m and 633vs.

[$CuCl_2$(bipy)] 2a. Reagent: $CuCl_2 \cdot 2H_2O$. Yield 78% (Found: C, 41.30; H, 2.70; N, 9.50. Calc. for $C_{10}H_8Cl_2CuN_2$: C, 41.30; H, 2.75; N, 9.65%). The cyan complex displays μ_{eff} = 1.81 μ_B at 294 K. Main 4,4′-bipyridyl IR bands (cm^{-1}): 1608vs, 1491s, 1417vs, 1217vs, 1080s, 1017s, 813vs, 730m and 646s. Freshly prepared powders belong to the α phase (orthorhombic), while ageing at room temperature affords increasing amounts of a monoclinic phase (β) with similar cell parameters. The latter can be selectively produced by pressing the powder in a pelletizer, for 5 h at 1 GPa.

Structure analysis

X-Ray powder diffraction data were taken with Cu-Kα radiation (λ = 1.5418 Å) on a Rigaku D-III MAX horizontal-scan powder diffractometer equipped with parallel Soller slits, a curved pyrolitic graphite monochromator in the diffracted beam, a Na(Tl)I scintillation counter and pulse height amplifier discrimination. The generator was operated at 40 kV and 40 mA. Slits used: (divergence slit) 1.0, AS (antiscatter slit) 1.0, RS (receiving slit) 0.3°.

The powders were gently ground in an agate mortar, then deposited, with aid of a binder (5% collodion in amyl acetate) on a zero-background plate (Si 511 monocrystal, supplied by The Gem Dugout, State College, PA), and rotated at about 60 rpm about the scattering vector in order to reduce the effects of preferred orientation. The data were collected, at room temperature, in the 5–90° (2θ) range, in the θ–2θ mode, step scan with Δ(2θ) = 0.02° and fixed time = 10 s, each entire run lasting about 12 h. Fig. 1 shows the raw X-ray powder diffraction (XRPD) data.

Standard peak-search methods were used for location of the diffraction maxima, which were then fed to the trial-and-error indexing program TREOR.[19] In the cubic, hexagonal, trigonal or tetragonal crystal systems no solutions were found. The results of the indexing procedure and the relative figures of merit are collected in Table 1. From the values reported we easily detected the isomorphous character of compounds **1a**, **1b** and **2a** (α). The solution of the structures of these three compounds was first originally performed on the [{$NiCl_2$(bipy)}$_n$] derivative; its space group was chosen as centric *Cmmm* from the analysis of systematic absences (only the *hkl*, $h + k = 2n$ condition was evidenced) and subsequently confirmed by a satisfactory refinement, not requiring a lowering of the symmetry into any acentric subgroup. The ALLHKL[20] program was used to extract integrated intensities for 45 space group-allowed reflections in the 2θ 5–55° range. These were then used in the direct methods package specifically developed for powder data, SIRPOW,[21] which, after a few cycles, provided the initial atomic coordinates for Ni and Cl and an $R(F^2)$ factor of 0.122%. At this stage, the (expected) polymeric nature of the compound was clear. The missing atoms of the 4,4′-bipyridyl ligand were then added in ideal positions as a starting model. The same model was then used for the two other isomorphous compounds.

The starting structural model for the (monoclinic) [{$CuBr_2$(bipy)}$_n$] complex was taken from the refined values of the orthorhombic structures of **1a**, **1b** and **2a** (α), as it was observed that the lattice metrics and systematic absences were consistent with the *C*2/*m* space group, which is a proper subgroup of *Cmmm*. The chemical nature of this symmetry change is described in detail in the following section.

The structure of the β (monoclinic) [{$CuCl_2$(bipy)}$_n$] phase was determined by observing that the lattice metrics of a non-conventional *C*2/*m* (*c* unique) setting (obtained by transforming the original monoclinic cell found by TREOR by the [1, 0, −1; −1, 0, −1; 0, 1, 0] matrix, see Table 1) closely match those of the α phase, from which approximate coordinates were taken. Again *C*2/*m* (*c* unique) is a proper subgroup of *Cmmm*,

Table 1 Lattice parameters for compounds **1a**, **1b**, **2a** (α and β) and **2b** as determined by the trial-and-error indexing program TREOR[19]

Compound	a/Å	b/Å	c/Å	β/°	U/Å^3	F^a	M^a	N_{obs}
1a [{$NiCl_2$(bipy)}$_n$]	12.049	11.323	3.589		489	50 (0.0088, 32)	41	11
1b [{$NiBr_2$(bipy)}$_n$]	12.464	11.329	3.738		528	20 (0.0225, 25)	21	11
2a α-[{$CuCl_2$(bipy)}$_n$]	12.123	11.121	3.756		506	21 (0.0160, 30)	27	10
2a β-[{$CuCl_2$(bipy)}$_n$]	8.342	3.739	8.059	95.0	251	45 (0.0128, 19)	80	11
	12.094	*11.082*	*3.739*	*91.98* (γ)[b]	502			
2b [{$CuBr_2$(bipy)}$_n$]	12.313	11.116	3.972	98.8	536	16 (0.0192, 63)	12	19

[a] F and M are DeWolff and Smith's figures of merit,[19] respectively, for powder pattern indexing; values greater than 20 *and* absence of unindexed peaks are typically taken as strong indication of correct indexing. [b] After transformation into non-standard setting of $C2/m$ (c unique).

although a different set of symmetry operations than for the bromide derivative must be removed, since the **2b** and **2a** (β) phases, in spite of sharing similar lattice parameters and the same space group (see Table 1), are *not* isomorphous.

The four structures were ultimately refined using the Rietveld technique and the GSAS[22] package on a Silicon Graphics Indigo computer. In the final runs the low-angle data, *i.e.* those affected most by instrumental aberrations, were discarded. A detailed description of the experimental procedure and data analysis can be found in ref. 17.

All four patterns showed a remarkable anisotropy of the diffraction peak widths, which need to be modelled, in the reciprocal space, by a vectorial, rather than a scalar (θ), quantity (for a structural interpretation of this effect, see Results and Discussion). This is particularly evident for the powder diffraction patterns of compound **2a** (α and β). Therefore, several refinement procedures with different analytical expressions were performed, using (*i*) a locally modified version of Young's code,[15] (*ii*) Scardi's microstructural analysis technique[23] and (*iii*) Bérar's program.[24] Unsatisfactory, and sometimes unstable, results were obtained; finally the anisotropic broadening axis option (which, on using a negative coefficient, allows empirical modelling of the sharp $0k0$ reflections) of GSAS[22] was chosen. The complex and awkward modelling of the diffraction peaks is, obviously, reflected in the rather high R_F agreement factors of the **2a** (α and β) phases (see Table 2); because the highly fluorescent radiation of the copper atoms of **2a** and **2b** heavily increases the background levels, profile R_p factors hide, in these two patterns, the still imperfect match. With such poorly crystallized materials, more than ever, it's the soundness of the chemical models (and the direct inspection of the matched patterns) which gives confidence to the results presented.

All bond distances and angles within the aza-aromatic rings were set at 1.38 Å and 120°, respectively; since this was achieved by imposing stiff chemical restraints by adding 'geometrical' observational equations, the final estimated standard deviations of the carbon and nitrogen atoms are biased, and should be considered as rather underestimated; obviously, this is not the case for the halogen atoms, resulting in statistically sound estimated standard deviations (e.s.d.s) in their refined coordinates and bonding parameters.

A single overall isotropic thermal parameter was refined and the contribution of the hydrogen atoms to the structure factors neglected. Atomic scattering factors were taken from the internal library of GSAS. Final R_p, R_{wp} and R_F values are reported in Table 2. Figs. 2 and 3 show the observed and calculated diffraction patterns for compounds **1a**, **1b** and **2a** (α and β) and **2b**, respectively. Crystal data and details on the refinements are collected in Table 2. Final fractional atomic coordinates for the compounds are reported in Tables 3 and 4.

Results and Discussion

All five structures will be discussed with a common reference frame, *i.e.* that derived from stacking (along a) of layers defined, in the bc plane, by a short period (c, the M–X–M interactions, X = Cl or Br) and a longer 'rod' axis (b, the M–bipy–M one). Relevant geometrical parameters for all five compounds are collected in Table 5.

The crystalline structures of the nickel derivatives **1a** and **1b** are based on a two-dimensional framework built by NiX_2 (X = Cl or Br) chains (similar to those found in the aristotypic α-$PdCl_2$ structure), connected by bidentate 4,4′-bipyridyl rods, which occupy the axial positions of the *trans*-D_{4h} octahedrally co-ordinated metal atoms (see Fig. 4). Such two-dimensional layers stack in space by the lattice C-centring symmetry operation and weakly interact by van der Waals contacts (see Fig. 5). The Ni–X and Ni–N bonding distances (see Table 5) are in the normal range found for similar compounds and mainly reflect the different sizes of the halides, allowing a slightly shorter Ni–N distance [2.114(4) *vs.* 2.128(4) Å] for the less sterically hindered environment of the chlorine derivative.

Ideally, [{$CuBr_2$(bipy)}$_n$] belongs to the same structural family as the nickel compounds, with the sole exception of the expected symmetry lowering of the $CuBr_4N_2$ chromophore by the presence of the Jahn–Teller distortion of d^9 ions. Two *trans* bromide ions are now at much shorter distances than the others [2.442(2) *vs.* 3.195(3) Å], making the copper atoms four- rather than six-co-ordinated (see Fig. 6). This effect, in turn, lowers the space group symmetry to monoclinic $C2/m$. Therefore, strictly speaking, there is no direct bond between neighbouring copper ions along a, and the full structure is ideally built from one-dimensional rods of 2/mL beam symmetry,[26] with loose contacts between the metals and their axial bromide ligands. Moreover, the lower crowding of ligands about the metal atoms is also responsible for the significant shortening of the Cu–N bond distances [2.075(8) *vs.* 2.128(4) Å for six-coordinated Ni^{II} of **1b**] as well of the M–Br bond distances [2.442(2) *vs.* 2.595(1) Å in **1b**].

From the previous observations and the recent report of the similar lattice parameters of the [{CuX_2(pyz)}$_n$] (X = Cl or Br) phases (monoclinic $C2/m$),[14] one would expect that the chloride analogue of [{$CuBr_2$(bipy)}$_n$] should be isomorphous to compound **2b** and crystallize in monoclinic $C2$ m with evident Jahn–Teller distortion. Unexpectedly, two different crystal phases of [{$CuCl_2$(bipy)}$_n$] were prepared, none fulfilling the above expectations. Therefore, [{$CuCl_2$(bipy)}$_n$] is an outlier. Indeed, as discussed later, the orthorhombic (α) phase possesses lattice metrics similar to those of the nickel compounds, but contains a (disordered) $MN_2X_2X'_2$ chromophore strongly perturbed by Jahn–Teller distortion. On the contrary, the β phase is truly monoclinic, as is the ordered copper bromide derivative, but not isostructural to it, since the β phase is disordered and its monoclinic angle is γ.

The α phase could only be satisfactorily refined by a split-chlorine atom model in space $Cmmm$, with site occupancy 0.50. A corresponding splitting of some bipyridyl atoms, in order to check whether the organic ligand does not lie on the crystallographic mirror plane normal to c, worsened the overall fit. Within this description, each layer, the bc plane, is built from one-dimensional rods equivalent to those found in compound

Table 2 Crystal data for compounds **1a**, **1b**, **2a** (α and β) and **2b**

Compound	$[\{NiCl_2(bipy)\}_n]$	$[\{NiBr_2(bipy)\}_n]$	α-$[\{CuCl_2(bipy)\}_n]$	β-$[\{CuCl_2(bipy)\}_n]$	$[\{CuBr_2(bipy)\}_n]$
Formula	$C_{10}H_8Cl_2N_2Ni$	$C_{10}H_8Br_2N_2Ni$	$C_{10}H_8Cl_2CuN_2$	$C_{10}H_8Cl_2CuN_2$	$C_{10}H_8Br_2CuN_2$
M	285.80	374.71	290.63	290.63	374.54
Crystal system	Orthorhombic	Orthorhombic	Orthorhombic	Monoclinic	Monoclinic
Space group	*Cmmm*	*Cmmm*	*Cmmm*	*C2/m* (*c* unique)	*C2/m* (*b* unique)
a/Å	11.9822(9)	12.3955(4)	12.104(2)	12.111(2)	12.291(1)
b/Å	11.3196(6)	11.3298(3)	11.140(4)	11.117(3)	11.1302(9)
c/Å	3.5830(3)	3.7338(1)	3.752(1)	3.754(1)	3.9747(4)
β,γ/°	—	—	—	92.08(1)	99.653(4)
U/Å^3	485.98(6)	524.37(3)	505.9(3)	505.1(2)	536.04(8)
D_c/g cm^{-3}	1.953	2.373	1.908	1.911	2.351
F(000)	288	360	290	290	362
μ/cm^{-1}	77.35	114.03	76.98	77.17	114.08
Scan range/°	17 < 2θ < 90	17 < 2θ < 90	17 < 2θ < 90	20 < 2θ < 90	17 < 2θ < 90
No. observations	3651	3651	3651	3501	3651
No. reflections	271	290	284	497	465
R_p	0.091	0.062	0.041	0.038	0.037
R_{wp}	0.120	0.081	0.052	0.054	0.051
R_F	0.067	0.044	0.119	0.091	0.041

$R_p = \Sigma|y_i - y_{ci}|/\Sigma y_i$, $R_{wp} = [\Sigma w_i(y_i - y_{ci})^2/\Sigma w_i y_i^2]^{\frac{1}{2}}$, $R_F = \Sigma|F_o - F_c|/\Sigma F_o$, where y_i and y_{ci} are the observed and calculated intensities at the ith step, respectively, w_i is a weighting factor (taken as $w_i = 1/y_i$) and F_o and F_c are the 'observed' and calculated structure factors for all the allowed reflections. For all structures, $Z = 2$ and scan mode is θ–2θ.

Table 3 Fractional atomic coordinates (e.s.d.s in parentheses) for compounds **1a** (first row) and **1b** (second row)

	X/*a*	*Y*/*b*	*Z*/*c*
Ni	0	0	0
	0	0	0
X	0.140 9(2)	0	0.5
	0.145 4(1)	0	0.5
N	0	0.186 6(3)	0
	0	0.188 5(3)	0
C(1)	0.099 68(7)	0.247 4(3)	0
	0.096 41(4)	0.249 3(3)	0
C(2)	0.099 56(7)	0.369 8(3)	0
	0.096 32(4)	0.372 4(2)	0
C(3)	0	0.432 2(3)	0
	0	0.433 2(2)	0

Table 4 Fractional atomic coordinates (e.s.d.s in parentheses) for compounds **2a** (α) (first row), **2a** (β) (second row) and **2b** (third row)

	X/*a*	*Y*/*b*	*Z*/*c*
Cu	0	0	0
	0	0	0
	0	0	0
X	0.150 1(5)	0	0.396(2)
	0.150 7(6)	0.006 1(5)	0.384(1)
	0.161 9(2)	0	0.449 7(6)
N	0	0.184 1(4)	0
	0.002(1)	0.185 3(3)	0
	0	0.186 7(6)	0
C(1)	0.098 73(5)	0.246 0(4)	0
	0.095(1)	0.254(1)	0.089(6)
	0.090 3(3)	0.247 5(6)	−0.072(2)
C(2)	0.098 62(6)	0.370 0(4)	0
	0.091(2)	0.378(1)	0.101(5)
	0.087 6(4)	0.372 2(6)	−0.092(2)
C(3)	0	0.432 7(3)	0
	−0.005(2)	0.433 2(2)	0
	0	0.435 3(5)	0
C(4)	—	—	—
	−0.097(1)	0.364(1)	−0.095(6)
	—	—	—
C(5)	—	—	—
	−0.095(1)	0.240(1)	−0.084(5)
	—	—	—

2b, possessing local 2/*m* (rather than *mmm*) symmetry at the copper atoms and two short [2.370(5) Å] and two long [2.884(7) Å] Cu–Cl interactions. The observed disorder can in principle be attributed to loss of correlation, along *b*, of the directions of the Cl–Cu–Cl vectors, as depicted in Scheme 1. However, it is also possible that a rigorously crystalline order along *b* occurs, and is accompanied by a disordered stacking of the layers along *a*. X-Ray powder diffraction could in principle distinguish between the two models by analysing the peak widths in the vector space. In the present case the sharpest peaks are the 0*k*0 ones; this suggests a rigorous crystalline order along *b* (the rod axis) and loss of coherence normal to it. However, the complex diffraction pattern does not allow one to discriminate between the shapes of the (broad) *h*00 and 00*l* peaks, hence between the two above-mentioned disorder models or their co-presence.

The occurrence and the nature of the β phase of $[\{CuCl_2(bipy)\}_n]$ is more difficult to explain. For sake of simplicity, its structure has been refined and presented, both in Tables 2 and 5), in the non-standard *C*2/*m* (*c* unique) space group, which allows direct and useful comparison of coordinates and packing modes. Table 5 shows that the major differences in the bonding parameters at the metal centres occur at the loosely bound Cl ions, for which an increase of 0.06 Å in the Cu · · · Cl contact is observed. The nature of the monoclinic symmetry, in this case, cannot be explained by the presence of the Jahn–Teller effect as in compound **2b**, since a split-atom model for Cl was still necessary to fit the observed intensities (the mirror plane perpendicular to *c* being still present and requiring the interpretation of the disorder *exactly* as in the α phase). Moreover, in this case, the bipyridyl ligand was eventually refined off-plane (disordered) and resulted in Cl–Cu–N–C angles similar to those found in the bromide derivative (see Table 5). Given that it is the γ angle which now differs from 90°, the interpretation of such a symmetry lowering, which is spontaneous upon ageing ($t_{\frac{1}{2}}$ = a few months!) or under pressure (see Experimental section), needs a crystallochemical analysis of the packing in the *ac* plane. Our data suggest that the (still disordered) β phase is more stable, at room temperature, than α-$[\{CuCl_2(bipy)\}_n]$ and, possessing a slightly higher density, can be selectively produced by applying a pressure of 1 Gpa to powders of the α phase. Indeed, as evidenced by the pertinent X–Cu–N–C angles, the nature of this process involves a reorientation of the 4,4′-bipyridyl ligand about its rod axis, which requires only small shifts of atoms toward a denser packing. This slight reorientation of the organic ligand, even if concurrent with the change of the γ angle, should only affect β (as in **2b**); hence, we tentatively

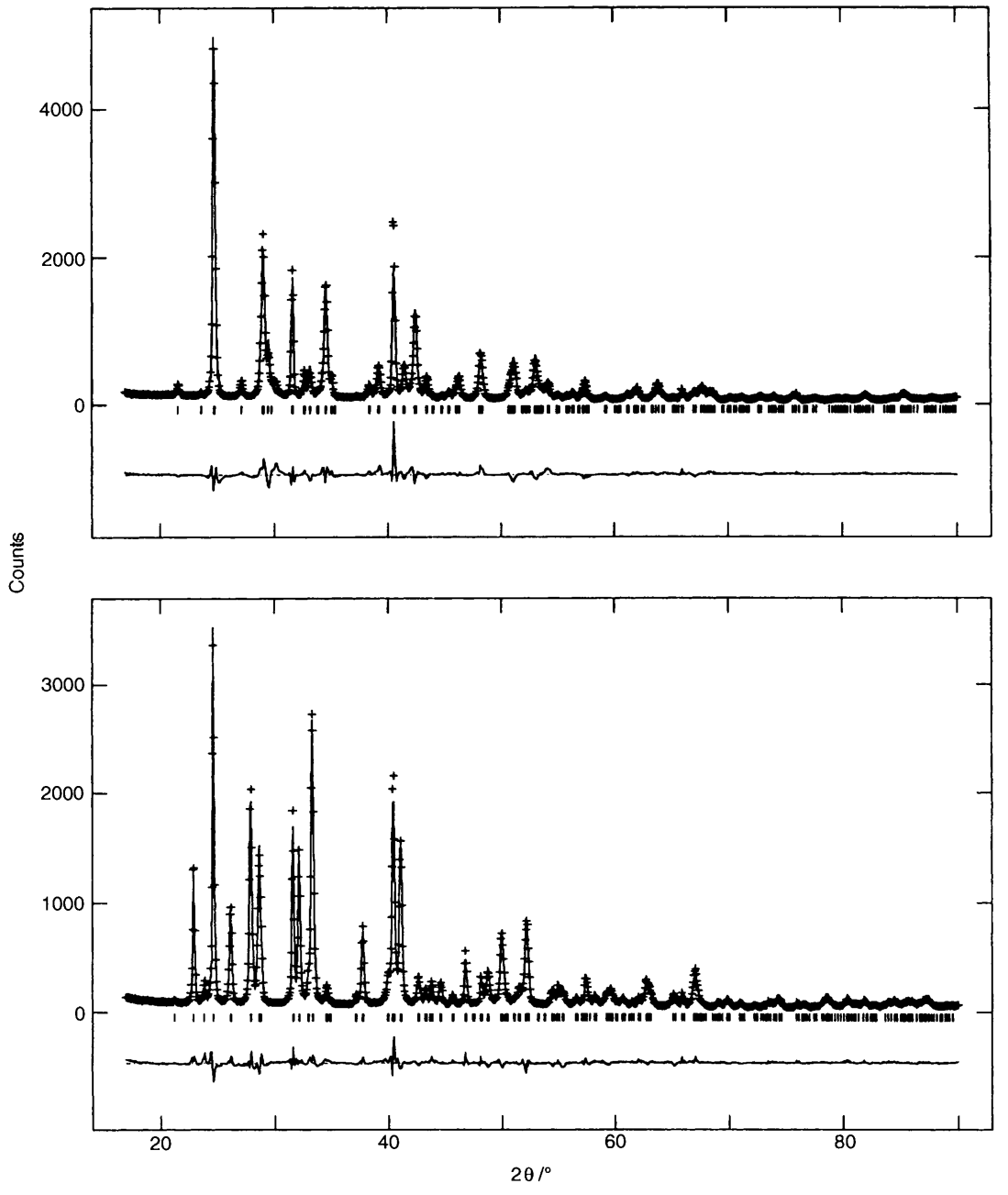

Fig. 2 Final Rietveld refinement plots for compounds **1a** (top) and **1b** (bottom); including peak markers and difference plot

Table 5 Relevant bond distances (Å) and angles (°) for compounds **1a**, **1b**, **2a** (α and β) and **2b**

	$[\{NiCl_2(bipy)\}_n]$ **1a**	$[\{NiBr_2(bipy)\}_n]$ **1b**	α-$[\{CuCl_2(bipy)\}_n]$ **2a** (α)	β-$[\{CuCl_2(bipy)\}_n]$ **2a** (β)	$[\{CuBr_2(bipy)\}_n]$ **2b**
M	Ni	Ni	Cu	Cu	Cu
X	Cl	Br	Cl	Cl	Br
M–X	(4 ×) 2.461(2)	(4 ×) 2.595(1)	(2 ×) 2.370(5) (2 ×) 2.884(7)	(2 ×) 2.324(6) (2 ×) 2.946(6)	(2 ×) 2.442(2) (2 ×) 3.195(3)
X–M–X	180, 93.41(9)	180, 92.00(4)	180	180	180
M–N	2.114(4)	2.128(4)	2.051(3)	2.059(3)	2.075(8)
X–M–N–C	46.70(4)	46.01(2)	39(1)	54(1)	60.1(4)

attribute the observed formation of the monoclinic (*c* unique) phase to a shearing mechanism leading to a slightly different stacking vector [in **2a**(β), the *a* parameter is *not* normal to *b*] of the layers along *a*; this, in turn, is in agreement with the extreme anisotropy of the peak widths in **2a**(β), which has been only partially accounted for, as explained in the Experimental section by a complex model. Why this effect does not occur in the bromine derivative **2b** is still unknown, but can be probably attributed to interlayer co-operation of the bulkier (protruding) anions in driving uniquely the crystallization to the monoclinic *ordered* phase.

The thermal properties of the five crystalline phases were also studied with the aid of TGA analyses. We found that the nickel complexes **1a** and **1b** are rather stable, and decompose above 420 °C. The decomposition processes are complex; however, in both cases, two main events can be observed, *i.e.* the subsequent

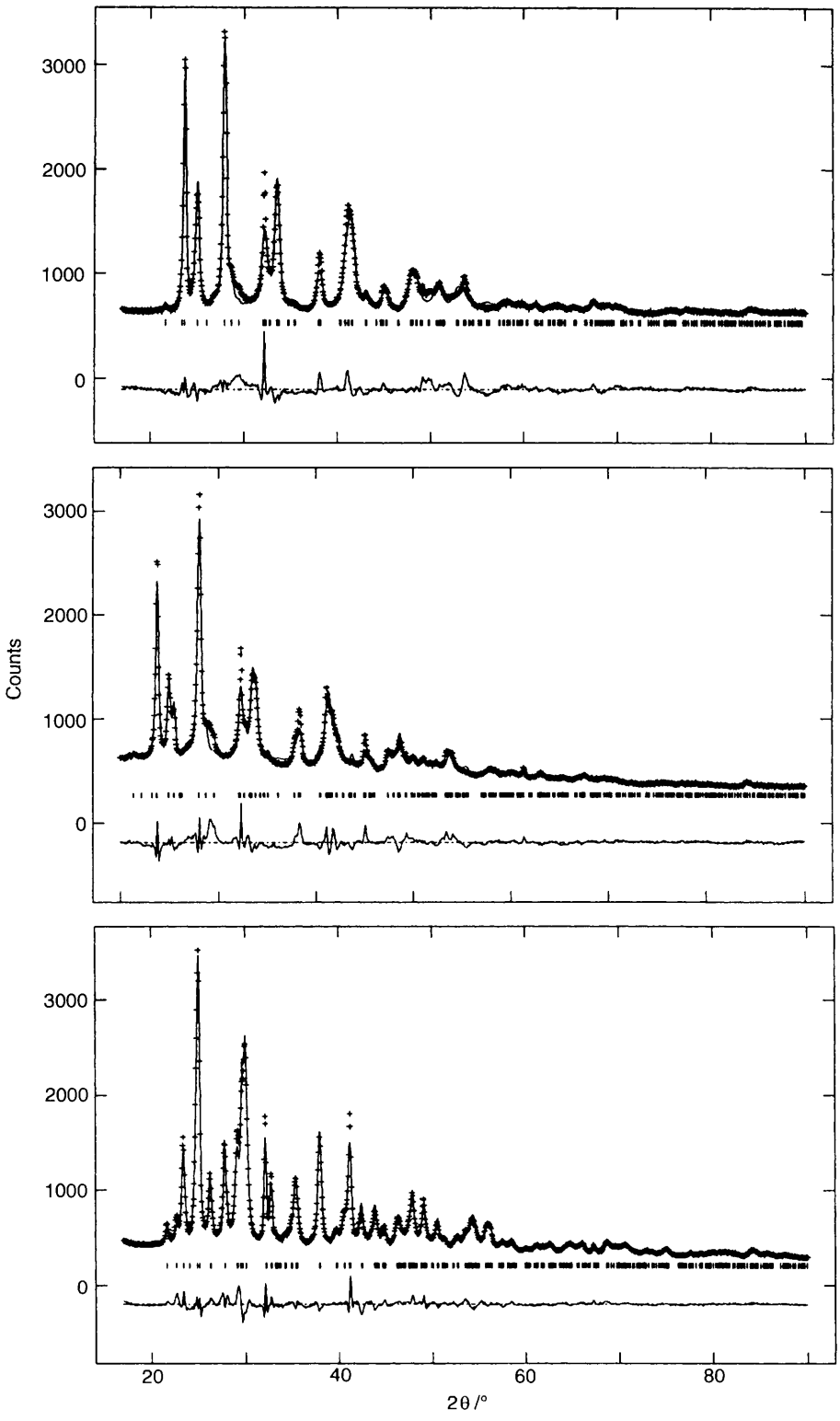

Fig. 3 Final Rietveld refinement plots for compounds **2a**(α) (top), **2a**(β) (middle) and **2b** (bottom); including peak markers and difference plot

loss of the 4,4′-bipyridyl ligand and of the halogen atoms, leaving a black residue, at $T > 600$ °C, of metallic nickel. Powders of **2a** (from a thermal point of view, the α and β phases appeared indistinguishable), when heated, suddenly lose the organic ligand slightly above 320 °C in a very narrow temperature range, generating $CuCl_2$ which is stable up to about 600 °C.

A slightly different thermal behaviour was observed for the bromine analogue **2b** since loss of the 4,4′-bipyridyl ligand at about 310 °C is accompanied by loss of bromine, possibly generating the copper(I) salt CuBr and leading, with a rather continuous slope in the TGA trace, to copper metal at $T > 650$ °C. In order better to understand this discrepancy among the **2a** and **2b** phases, we run a TGA experiment also on pure $CuBr_2$, which showed sudden formation of the CuBr phase, by loss of half a mole of Br_2, at about 190 °C. Coupling the above observations, we can attribute the complex decomposition pattern of **2b** to the intrinsic instability of $CuBr_2$ at elevated temperatures; however, it is evident from the higher decomposition temperature of **2b** that stabilization of the $CuBr_2$ fragment by the organic ligand occurs.

Finally, our measurements lead to the observation that the

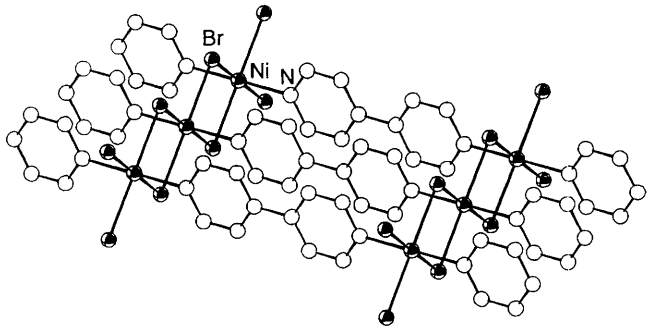

Fig. 4 An ORTEP[25] drawing of a two-dimensional layer, normal to *a*, of the $[\{NiBr_2(bipy)\}_n]$ **1b** phase; the chloride derivative **1a** is strictly isostructural

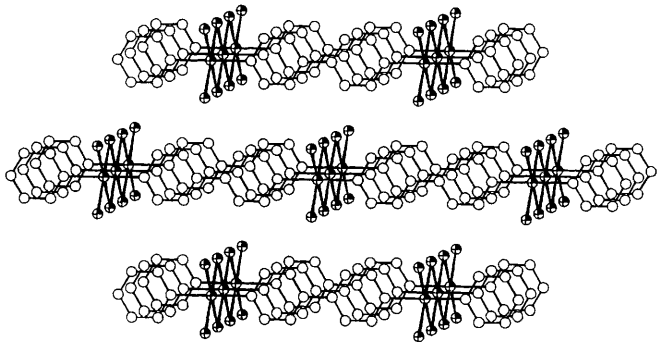

Fig. 5 Packing diagram of $[\{NiBr_2(bipy)\}_n]$ **1b**, viewed approximately down *c*. Stacking occurs along *a*, while the rod axes coincide with *b*

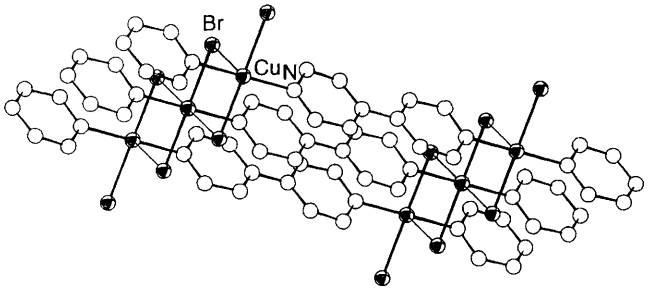

Fig. 6 an ORTEP drawing of a two-dimensional layer, normal to *a*, of the $[\{CuBr_2(bipy)\}_n]$ **2b** phase; thin solid lines depict long (Jahn–Teller distorted) Cu · · · Br interactions

nickel compounds, which are stable at much higher temperatures than the copper complexes, may not have easy decomposition paths through an unlikely nickel(I) intermediate.

Conclusions

The presented work is based on the crystal structure determination of several microcrystalline phases not easily obtainable as single crystals of suitable quality. Possibly, prolonged efforts and non-standard crystallization techniques would afford, in principle, such suitable crystals, thus putting into shade the above-mentioned results. However, when a crystalline phase results only from a solid-state transformation [such as **2a**(β)] it is likely that single crystals will never be grown and that powder diffraction will remain the ultimate tool for structural characterization.

In addition, we have shown that two-dimensional frameworks can easily be built by the simultaneous use of metal-bridging halides and long-period bifunctional bases. However, a different (three-dimensional) structural motif has been observed in the $Cd(CN)_2$ adducts of pyrazine or 1,4-bis(4-pyridyl)butadiyne,[27] due to the different co-ordination mode of

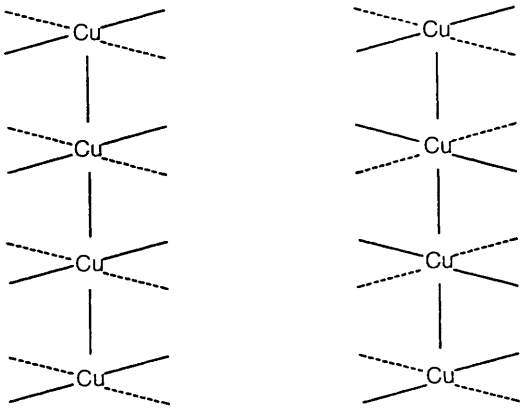

Scheme 1

the bridging cyanides (*vs.* halides), which affords folded CdX_2 sheets of squares. Nevertheless, the reported structures can be related to lighter homologues such as $[\{CuX_2(pyz)\}_n]$ (X = Cl or Br),[14] possessing shorter linear ambidentate amines. This could shed some light on the structural features of $[\{MX_2(L\text{–}L)\}_n]$ phases, where L–L indicates a generic spacer of pseudo-cylindrical symmetry.

Acknowledgements

We thank the Italian Consiglio Nazionale delle Ricerche (Progetto Finalizzato: Materiali Speciali per Tecnologie Avanzate) for funding.

References

1 See, for example, W. Kobel and M. Hanack, *Inorg. Chem.*, 1986, **25**, 103.
2 (*a*) A. B. Blake and W. E. Hatfield, *J. Chem. Soc., Dalton Trans.*, 1978, 868 and refs. therein; (*b*) J. A. Real, G. De Munno, M. C. Munoz and M. Julve, *Inorg. Chem.*, 1991, **30**, 2701 and refs. therein; (*c*) Z. N. Chen, D. G. Fu, K. B. Yu and W. X. Tang, *J. Chem. Soc., Dalton Trans.*, 1994, 1917; (*d*) S. Kawata, S. Kitagawa, M. Kondo, I. Furuchi and M. Munakata, *Angew. Chem., Int. Ed. Engl.*, 1994, **33**, 1759.
3 O. Jung and C. G. Pierpont, *J. Am. Chem. Soc.*, 1994, **116**, 2229.
4 M. Fujita, Y. J. Kwon, S. Washizu and K. Ogura, *J. Am. Chem. Soc.*, 1994, **116**, 1151.
5 F. Kubel and J. Strahle, *Z. Naturforsch., Teil B*, 1982, **37**, 272; R. W. Gable, B. F. Hoskins and G. Winter, *Inorg. Chim. Acta*, 1985, **96**, 151; M. Julve, M. Verdaguer, J. Faus, F. Tinti, J. Moratal, A. Monge and E. Gutierrez-Puebla, *Inorg. Chem.*, 1987, **26**, 3520; B. F. Abrahams, B. F. Hoskins and G. Winter, *Aust. J. Chem.*, 1990, **43**, 1759; C. Chen, D. Xu, Y. Xu and C. Cheng, *Acta Crystallogr., Sect. C*, 1992, **48**, 1231.
6 R. Robson, B. F. Abrahams, S. R. Batten, R. W. Gable, B. F. Hoskins and J. Liu, *Supramolecular Architecture, American Chemical Society*, Washington, DC, 1992, ch. 19; S-X. Liu, *Acta Crystallogr., Sect. C*, 1992, **48**, 22.
7 R. W. Gable, B. F. Hoskins and R. Robson, *J. Chem. Soc., Chem. Commun.*, 1990, 1677.
8 L. R. MacGillivray, S. Subramanian and M. J. Zaworotko, *J. Chem. Soc., Chem. Commun.*, 1994, 1325.
9 L. Carlucci, G. Ciani, D. M. Proserpio and A. Sironi, *J. Chem. Soc., Chem. Commun.*, 1994, 2755.
10 T. Soma, H. Yuge and T. Iwamoto, *Angew. Chem., Int. Ed. Engl.*, 1994, **33**, 1665; F. Robinson and M. J. Zaworotko, *J. Chem. Soc., Chem. Commun.*, 1995, 2413; O. M. Yaghi and H. Li, *J. Am. Chem. Soc.*, 1996, **118**, 295.
11 T. R. Musgrave and C. E. Mattson, *Inorg. Chem.*, 1968, **7**, 1433.
12 J. R. Ferraro and K. C. Davis, *Inorg. Chim. Acta*, 1969, **3**, 685.
13 F. D. Ayres, P. Pauling and G. B. Robertson, *Inorg. Chem.*, 1964, **3**, 1303.
14 T. Fetzer, A. Lentz and T. Debaerdemaeker, *Z. Naturforsch., Teil B*, 1989, **44**, 553.
15 N. Masciocchi, M. Moret, P. Cairati, F. Ragaini and A. Sironi, *J. Chem. Soc., Dalton Trans.*, 1993, 471.
16 N. Masciocchi, P. Cairati, L. Carlucci, G. Ciani, G. Mezza and A. Sironi, *J. Chem. Soc., Dalton Trans.*, 1994, 3009.

17 N. Masciocchi, M. Moret, P. Cairati, A. Sironi, G. A. Ardizzoia and G. La Monica, *J. Am. Chem. Soc.*, 1994, **116**, 7668.
18 N. Masciocchi, M. Moret, P. Cairati, A. Sironi, G. A. Ardizzoia and G. La Monica, *J. Chem. Soc., Dalton Trans.*, 1995, 1671.
19 P. E. Werner, L. Eriksson and M. Westdahl, *J. Appl. Crystallogr.*, 1985, **18**, 367.
20 G. S. Pawley, *J. Appl. Crystallogr.*, 1981, **14**, 357.
21 G. Cascarano, L. Favia and C. Giacovazzo, *J. Appl. Crystallogr.*, 1992, **25**, 310.
22 A. C. Larson and R. B. Von Dreele, LANSCE, Ms-H805, Los Alamos National Laboratory, New Mexico, 1990.
23 L. Lutterotti, P. Scardi and P. Maistrelli, *J. Appl. Crystallogr.*, 1992, **25**, 459.
24 J. F. Bérar and P. Garnier, National Institute of Standards and Technology Conference, Gaithersburg, 1992, Book of Abstracts, p. 29.
25 C. K. Johnson, ORTEP, Report ORNL-5138, Oak Ridge National Laboratory, Oak Ridge, TN, 1976.
26 J. B. Thompson jun., *Am. Mineral.*, 1978, **63**, 239.
27 B. F. Abrahams, M. J. Hardie, B. F. Hoskins, R. Robson and E. E. Sutherland, *J. Chem. Soc., Chem. Commun.*, 1994, 1049.

Received 7th February 1996; *Paper* 6/00895J